Theor Chem Acc (2011) 128:327–339
DOI 10.1007/s00214-010-0859-7

REGULAR ARTICLE

Thermolysis of 2-methyloxetane: a computational study

J. Martín-Ortiz · J. J. Quirante

Received: 7 June 2010 / Accepted: 12 November 2010 / Published online: 12 December 2010

Abstract Thermal fragmentation of 2-methyloxetane (2MO), which yields two different sets of products by virtue of ring asymmetry, was studied theoretically by using DFT, MPn and CASPT2//CASSCF methods. At the MPn and DFT theoretical levels, only concerted transition states were located on the ground state potential energy surface (PES). The CASSCF approach leads to different stepwise pathways for the two fragmentation modes, with biradical as intermediates, in addition to the concerted paths, with a very shallow PES for the asynchronous region in which intermediates becomes unstable under CASPT2// CASSCF calculations. Nevertheless, activation barriers thus calculated were quite consistent with experimental values. The reaction pathway that experimentally renders the main set of products was calculated as the lowest-energy path for the fragmentation of the 2-methyloxetane heterocycle, and this evolves with an initial cleavage of the C–O bond of the oxetane ring.

Keywords Methyloxetanes · Thermal fragmentation · DFT · CASPT2//CASSCF study

1 Introduction

In general, the chemistry of oxetanes has been scarcely studied despite their significance. The oxetane ring is present in a number of naturally occurring compounds with interesting therapeutic properties (e.g. taxol, oxetanocin, thromboxane A_2) and also in hydrocarbon oxidation intermediates. In addition, oxetanes are useful chemicals for synthesizing a variety of products by hydrogenolysis, thermolysis, nucleophilic attack and other reactions with appropriate substrates [1–9].

Moreover, the oxetane thermolytic cycloreversion is highly useful for synthetic purposes. Thus, it gives carbonyl–olefin formal metathesis products [7–9], also oxetane metathesis under mold *Photoinduced Electron Transfer* (PET) provides an effective tool for preparing new carbonyl–alkene pairs. The cycloreversion process under PET conditions has in fact aroused much interest over the last decade by virtue of its involvement in the photoenzymatic repair of DNA damage [10–28].

Specifically, the thermal decomposition of 2-methyloxetane in the gas phase, which was the subject of the present study, has been studied experimentally over the temperature range 660–760 K [29]. The process takes place via two different reaction pathways (see Scheme 1) one of which prevails over the other.

Oxetane thermolysis (and the reverse reaction) has also aroused interest in establishing whether it takes place in a concerted manner or in two steps involving cleavage of the two bonds to be broken—or their formation in the reverse reaction—which would require the presence of a biradical intermediate. However, attempts at answering this question have so far provided non-conclusive evidences because they seem consistent with both types of mechanisms [29–36].

Worth special note among the theoretical studies addressing the previous question are those of Robb et al. on the Paternò–Büchi reaction by use of CASSCF methods [37], which led to two different stepwise mechanisms for

J. Martín-Ortiz · J. J. Quirante (✉)
Departamento de Química Física,
Facultad de Ciencias,
Universidad de Málaga,
Campus de Teatinos s/n,
29071 Málaga, Spain
e-mail: quirante@uma.es

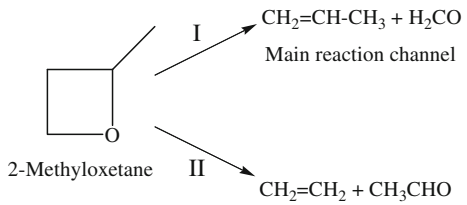

Scheme 1 Thermolysis of 2-methyloxetane

the process in the S_0 PES; and our own MP2, QCISD and DFT study of the thermolysis of 3-vinyloxetane [38], the results of which were consistent with concerted pathways, both synchronous and asynchronous—the latter, however, exhibited no biradical intermediates on the ground state PES.

The primary purpose of this work was to expand available theoretical knowledge about the reaction mechanism for the thermal decomposition of oxetanes. To this end, we studied 2-methyloxetane, asymmetric substitution in which affords the obtainment of two different sets of products via two different reaction pathways. Also, we rationalized the way the substituent dictates which pathway prevails for this compound.

2 Theoretical methods

While the theoretical study of reaction pathways potentially involving biradical species is known to require the use of wavefunctions with more than one Slater determinant—at least with CASSCF [39–41]—some authors have shown that the DFT, with a suitable choice of exchange–correlation functionals [42–46], and some post-HF correlated methods can also provide an accurate description for such species [47–54]. In this work, we used various chemical models constructed with theoretical tools ranging from the DFT ones (with the B3LYP [55–57] and MPW1K [58] functionals and both their restricted and unrestricted formalisms) to the CASPT2//CASSCF multi-configurational methods to take properly into account the dynamic correlation effects [59]. For comparison, we also used the MPn and QCISD correlated methods, and the G2 additive scheme (MP2, SVP) for highly precise energy predictions. All calculations were done with the Gaussian03 software package [60]—by exception, CASPT2 computations were obtained with MOLCAS v. 7.4 [61].

Singlet biradical exhibits generally two nearly degenerate potential energy surfaces (a type of avoided crossing situation) that requires of well-balanced theoretical methods to be adequately treated. Possible adverse results regarding its geometric localization can be obtained. The complete active space SCF (CASSCF) approach, which does not consider dynamical correlation contributions, may overestimate the stability of biradical on reaction pathways [44]. On the other hand, the DFT method that includes dynamical electronic correlation, in an unspecific manner, may not show the multi-reference character associated with non-dynamic or near degeneracy effects. The above-mentioned considerations should be of special relevancy with flat potential energy surfaces for the region of interest.

The most stable species in each case were completely optimized and transition states (TS) located by using the Schlegel algorithm [62] at various theoretical levels. All structures were optimized with the 6-31G(d) basis set. The nature of the different critical points on each PES was determined by IRC computations [63] done with the algorithm of González and Schlegel [64].

The active space used in the CASSCF calculations was that involving the Π and Π^* orbitals of the products in addition to the non-bonding *p* orbital of the oxygen atom: a total of six electrons in five orbitals. As this active space only includes a C–C bond and a C–O bond, there are two possible reference structures for the 2MO compound, each one corresponding to a definite fragmentation mode. Nonetheless, in this case, the two complementary active spaces gave identical geometries for 2MO and energies with a difference of only 0.1 kcal/mol (as represented in Fig. 7). CASPT2 computations required expanding the active space for improved wavefunction convergence. This involved introducing the orbitals of the carbon–oxygen bond in the carbonyl fragment and a 3*p* orbital of oxygen. An (8, 8) active space was thus considered.

Finally, electron rearrangement in the different reaction pathways were studied by examining the configurations of the wavefunctions for bimolecular transition states by means of a theoretical method originally developed by Fukui [65, 66]. This interpretative tool rewrites a TS monodeterminantal wavefunction (built in this work from the B3LYP/6-31G(d) Kohn–Sham Molecular Orbitals) as a combination of the electronic configurations of the interacting fragments,

$$\psi = C_0\psi_0 + \sum_q C_q\psi_q \qquad (1)$$

where ψ_0 is the reference state function in which neither electron transfer nor electron excitation takes place and ψ_q stands for monotransferred configurations (an electron of an occupied MO in any fragment is transferred to an unoccupied MO of a different one), monoexcited configurations (where the electron is excited to an unoccupied MO of the same fragment), ditransferred and so on. These contributions, under the assumption of fragment geometries being identical with that in the respective supermolecule structure, were estimated with the ANACAL program developed by López et al. [67–70] which has proven

usefulness for understanding the chemical features of complex formation and chemical reactivity [67–70].

3 Results and discussion

Scheme 2 shows the possible reaction pathways for the thermal decomposition of 2-methyloxetane. Both the concerted process I and the stepwise processes III and IV, which involve biradical intermediates, lead to formaldehyde and propene as products. On the other hand, the concerted mechanism II and the also stepwise reaction pathways V and VI give ethene and ethanal.

The asymmetric structure of the reagent allows the reaction pathways III to VI to be split into two different reaction pathways involving different conformational isomers of the previous intermediates. Scheme 3 shows the Newman type projections of the two rotamers of the biradical intermediates potentially formed by effect of the initial bond cleavage of 2-methyloxetane molecule. There are thus two conformational isomers for 2MO-INT_{III}, namely: a *gauche-in* isomer resulting from opening of the ring and placement of the oxygen atom on the same side as the methyl group, and a *gauche-out* isomer with the oxygen on the opposite side. Both species were examined on all the explored PES. 2MO-INT_{IV} can be formed from 2-methyloxetane with its methylene radical on the same (*gauche-in* conformer) or opposite side (*anti* rotamer) as the methyl substituent. Only the *anti* conformers in 2MO-INT_{IV} and 2MO-INT_{V}, which additionally include *gauche-in* conformers, were studied as they were subject to less steric hindrance. Finally, both rotamers for 2MO-TS_{VI} of the *gauche-in* type are equivalent.

3.1 Single-configuration methods

3.1.1 Concerted mechanisms I and II

Figure 1 shows the most salient structural data for all stationary points—reaction products excepted—identified on the explored PES [MP2/6-31G(d), B3LYP/6-31G(d) and MPW1K/6-31G(d)]. The geometries shown correspond to the B3LYP/6-31G(d) quantum model because our B3LYP and UB3LYP calculations provided identical results for these stationary points.

Application of the above-mentioned single-configuration MPn methods to the exploration of the asynchronous regions of the ground-state PES provided no evidence for the stepwise reaction pathways. With respect to DFT results, trials for the basic reaction of oxetane thermolysis [46], avoiding the spin and spatial symmetries by using the UB3LYP formalism (including the option GUES = MIX that requests that the HOMO and LUMO orbitals be mixed in the calculations), allow us to localize some transition states and biradical intermediates (for example, the analogous to 2MO-INT_{IV} and the analogues to 2MO-TS_{III} and 2MO-$TS_{III'}$ of Figs. 5 and 6, but no other points of those of the Scheme 2. These discouraged results and a lot of failed trials to localize point on the asynchronous region of PES for the 2MO fragmentation allow us to consider not suitable the UB3LYP method for the global study of reactivity of this system. Nonetheless, DFT results were very valuable in order to analyze the concerted mechanisms (see next section).

The transition states 2MO-TS_{I} and 2MO-TS_{II} (Fig. 1) corresponded to synchronous cleavage reactions in 2-methyloxetane. In both, the C–O bond was broken to a

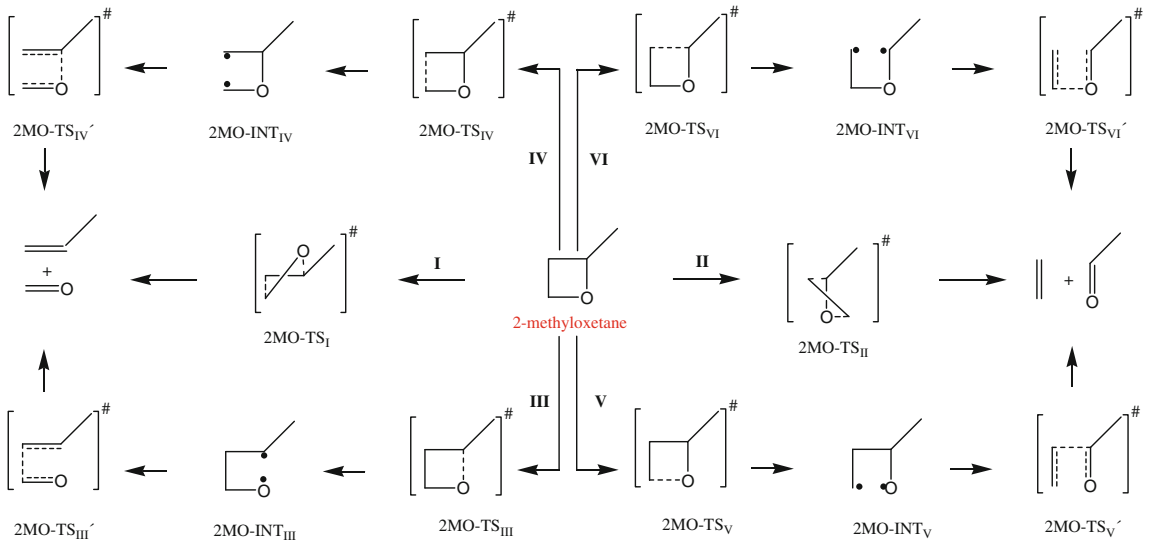

Scheme 2 Possible routes in the thermal decomposition of 2-methyloxetane

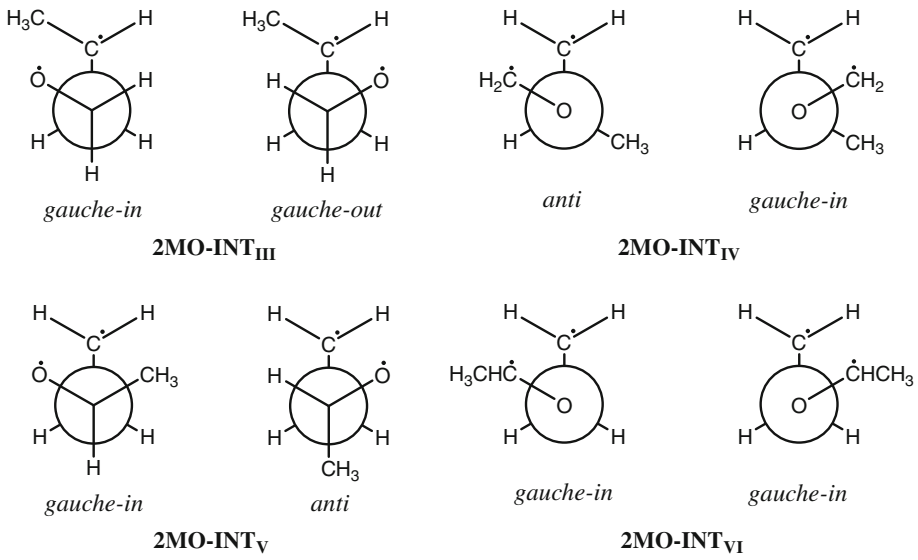

Scheme 3 Newman projections of the conformational isomers for the possible biradical intermediates that may form after a first bond cleavage in 2-methyloxetane. The terminology used, gauche-in/gauche-out/anti, describes the relative position of the methyl group in relation to one of the radical centers

slightly greater extent than the C–C bond; thus, the increase in C–O distance as calculated with the B3LYP functional was 0.831 Å in 2MO-TS$_I$ and 0.574 Å in 2MO-TS$_{II}$, whereas that in C–C was 0.191 Å in the former transition state and 0.454 Å in the latter.

Figure 2 shows the enthalpies of activation obtained with the above-described theoretical methods and the experimental values for comparison [29, 35]. Computations were done at the default temperature and pressure used by the Gaussian03 software package (298.15 K and 1.000 atm, respectively); in addition, G2 calculations were done at the temperature and pressure used to obtain the experimental data (700 K and 0.015 atm) (Table 1). All theoretical models used provided very similar energies of activation for both decomposition pathways. The energy of the transition state associated to pathway I was slightly lower than that for pathway II with all theoretical levels used except QCISD(T)-FC/cc-pVDZ//B3LYP/6-31G(d); this general result is consistent with a experimental $k_1^{(\infty)}/k_2^{(\infty)}$ ratio [29] which is temperature-dependent but invariably greater than unity.

Calculated mean unsigned errors (MUE parameter in the Table 1) were used to estimate the differences between theoretical and experimental enthalpies of activation. Holbrook et al. [35] obtained the same experimental energy of activation for both pathways (59.8 kcal/mol) and claimed that the only difference between the two in this respect was in the pre-exponential factor, *A*. On the other hand, Zalotai et al. [29] obtained different results for the two pathways; this led us to use their data set to calculate MUE here. As it was expected, we obtained the best MUE parameter for our G2 results.

3.1.2 *Configurational analysis of the wavefunction*

Table 2 shows the relative weights (as calculated from coefficients C_0 and C_q in Eq. 1) of the major electronic configurations of the fragments for the transition states 2MO-TS$_I$ and 2MO-TS$_{II}$ as computed with the B3LYP/6-31G(d) model, the net charge transfer between fragments—from B (the alkene) to A (the aldehyde) in all cases—and the calculated Mayer's interfragment bond orders [71, 72].

The increased weight of the zero AB configuration (A = ethanal, B = ethene) in the wavefunction for the transition state 2MO-TS$_{II}$ relative to the saddle point 2MO-TS$_I$, together with the Mayer bond orders values, indicates that 2MO-TS$_I$ (1.377) is more distant from the respective fragmentation products than is 2MO-TS$_{II}$ (1.204).

For the following discussion in this section, we consider the cycloaddition reverse processes (see Scheme 2): the most important electronic configuration between fragments—AB excluded—in both cases is that for a charge transfer from the alkene HOMO ($\Pi_{C=C}$) to the aldehyde LUMO ($\Pi^*_{C=O}$); however, the inductive effect of the methyl group in the alkene favors the electron release in 2MO-TS$_I$ with a net charge transfer twice greater than for 2MO-TS$_{II}$ (viz. 0.28*e* in 2MO-TS$_I$ and 0.15*e* in 2MO-TS$_{II}$). In addition, the transition states exhibit a slight secondary release from the aldehyde HOMO [*n* (2*p*O)] to the alkene LUMO ($\Pi^*_{C=C}$). The asynchronicity of the cycloaddition process, which favors formation of a C–C bond over a C–O bond in the two transition states (Fig. 1), and their geometric distortion (reflecting in the corresponding C_2–C_3–C_4–O_1 dihedral angles: 32.51° for 2MO-TS$_I$ and −27.36° for 2MO-TS$_{II}$), facilitate the electron transitions and, ultimately, a [2 *s* + 2 *s*] cycloaddition that is symmetry-forbidden in theory. The slight polarizing effects

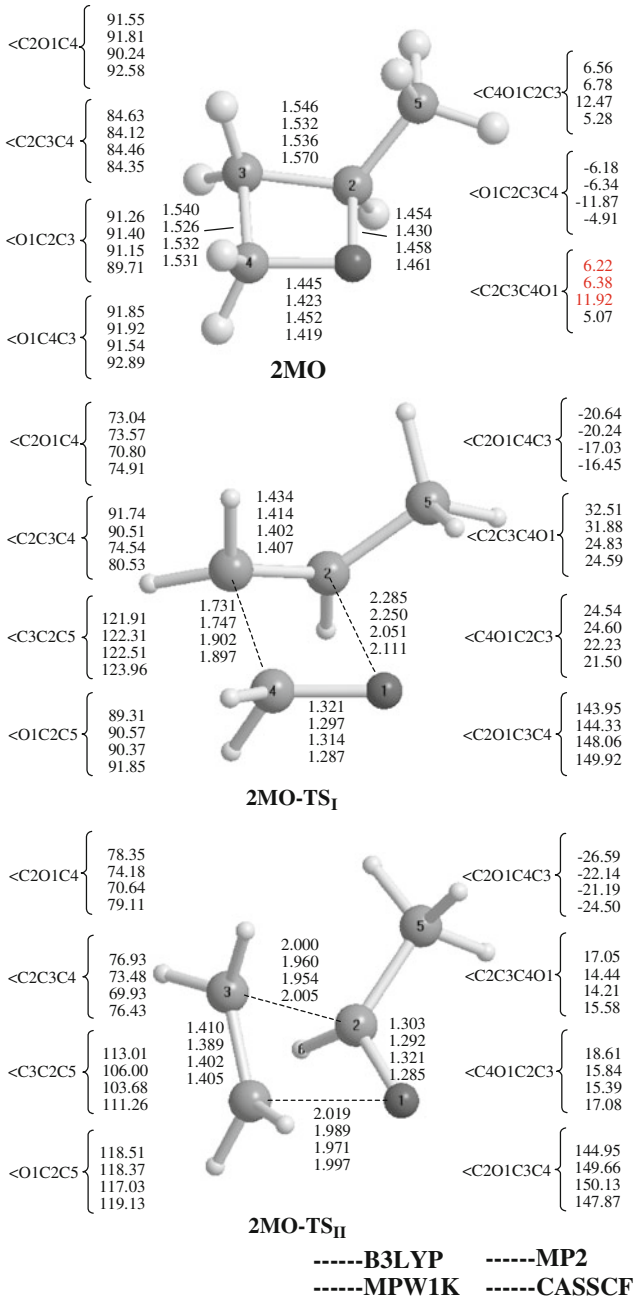

Fig. 1 Most important geometrical parameters of the stationary points located in the explored PESs with DFT, MP2 and CASSCF methods for the highly synchronous fragmentation of 2-methyloxetane. Bond distances are given in Å and angles in degrees

of fragment A (i.e. the A^*B configuration) result from single excitations on the aldehyde ($\Pi_{C=O} \rightarrow \Pi^*_{C=O}$ and n ($2p$O) $\rightarrow \Pi^*_{C=O}$), whereas those of fragment B (AB^* configuration), which are even smaller, are a consequence of single excitations in the alkene ($\Pi_{C=C} \rightarrow \Pi^*_{C=C}$). As a consequence of the above changes, there results a net stabilization of 2MO-TS_I against 2MO-TS_{II}, which is consistent with experimental evidences [29, 35].

Figure 3 illustrates the previous electron transfers and the corresponding electronic configurations, in addition to the variation of the energy of the frontier orbitals of the fragments when they adopt the supermolecule geometry of the TS. As can be seen, the energy of non-bonding orbitals decreases, whereas that of bonding orbitals increases and that of n ($2p$O) remains virtually unchanged. Also, the strongest interaction is that between the highest-energy HOMO (in the alkene) and the lowest-energy LUMO (in the aldehyde), the energy difference between the two orbitals being lower for 2MO-TS_I (i.e. the most stable transition state).

Based on the signs of the lobes of the p orbitals involved in the interaction leading to the major configuration (Fig. 4a) in both transition states, only that between a carbon atom in the alkene and another in the aldehyde is favorable—those between the other p orbitals are all unfavorable—as a result, the concerted cycloaddition process must be somewhat asymmetric starting with formation of the C–C bond. The transition states are stabilized by the other orbital interactions described above and depicted schematically in Fig. 4b, c. Torsion of the fragments about the C–C bond while it forms (see the C_2–C_3–C_4–O_1 dihedral angle for 2MO-TS_I and 2MO-TS_{II}) facilitates the favorable interaction depicted in Fig. 4c and hinders the unfavorable interaction between the oxygen and carbon atoms of Fig. 4a.

In addition and by comparison with similar results for the fragmentation of unsubstituted oxetane, we found that for 2MO-TS_I, the $+I$ inductive effect of the methyl group at position C2 reinforces the main interaction and not the secondary ones. For 2MO-TS_{II}, the effect is less pronounced because the transition state corresponds to a reaction where the methyl substituent does not belong to the olefin.

3.2 Multi-configuration methods

All species in Scheme 2 were located on the CASSCF(6,5)/6-31G(d) potential energy surface; by exception, the transition state 2MO-$TS_{III'}$ (*gauche-in*) only converged at slightly lower computational levels (with a basis set containing no polarization functions).

Figures 1, 5 and 6 show the most salient geometric parameters for the stationary points obtained at the CASSCF level, and Figs. 7 and 8 summarize the obtained reaction energy profiles.

3.2.1 Concerted mechanisms I and II

Regarding the transition states typical of concerted reactions, computations yielded the two species corresponding to pathways I and II in Scheme 2 (viz. 2MO-TS_I and

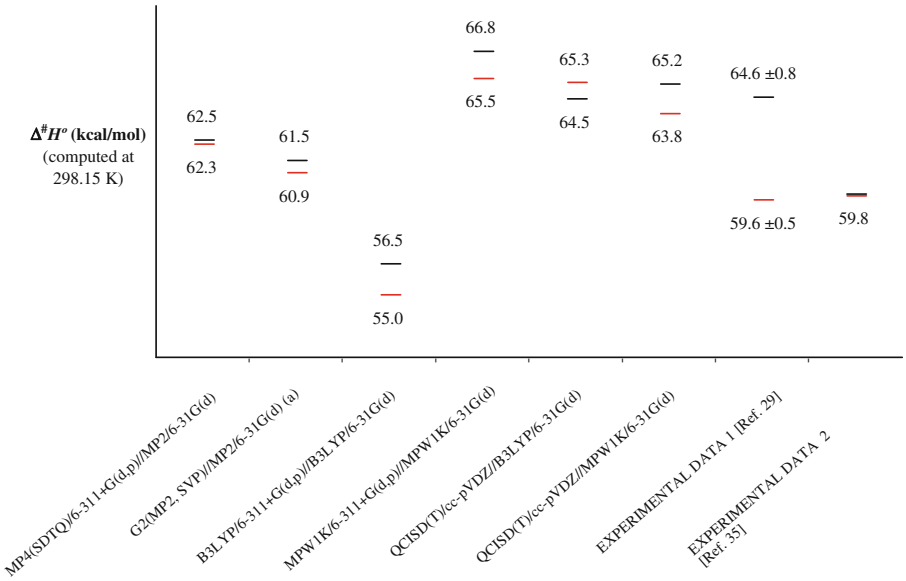

Fig. 2 Comparison between the standard activation enthalpies calculated at 298.15 K and the experimental values available. The *red lines* correspond to the 2MO-TS_I values and *black* ones to the 2MO-TS_{II}. **a** When it was calculated at 700.00 K and 0.015 atm. (conditions for experimental data), we were also obtained about these values

Table 1 *MUE* (mean unsigned error) parameter values

Theoretical level	$\Delta^{\#}H^{\circ}$ (kcal/mol)		*MUE*
	2MO-TS_I	2MO-TS_{II}	
MP4(SDTQ)/6-311 + G(d,p)//MP2/6-31G(d)	62.3	62.6	2.4
G2(MP2) 700 K 0.015 Atm	61.3	61.9	2.2
G2(MP2) 298.15 K 1.000 Atm	60.9	61.5	2.2
B3LYP/6-311 + G(d,p)//B3LYP/6-31G(d)	55.0	56.5	6.3
MPW1K/6-311 + G(d,p)//MPW1K/6-31G(d)	65.5	66.8	4.1
QCISD(T)/cc-pvDZ//B3LYP/6-31G(d)	65.3	64.5	2.9
QCISD(T)/cc-pvDZ//MPW1K/6-31G(d)	63.8	65.2	2.4
Experimental data 1 [Ref. 29]	59.6	64.6	0.0

Table 2 Relative weights for the most important fragment electronic configurations in the B3LYP/6-31G(d) transition structures 2MO-TS_I and 2MO-TS_{II}

Configurations	2MO-TS_I[a]	2MO-TS_{II}[b]
AB	1.000 (1.000)	1.000
$A^{-}B^{+}$	0.724 (0.507)	0.459
$A^{+}B^{-}$	0.277 (0.252)	0.253
$A^{-2}B^{+2}$	0.170 (0.093)	0.080
$AB^{*}/A^{*}B$	0.170/0.181 (0.133/0.192)	0.135/0.171
Net charge transfer	0.28e (0.20e)	0.15e
Mayer interfragment bond order	1.377 (1.206)	1.204

In parentheses are the values corresponding to the transition state for the oxetane thermolysis

[a] *A* H_2CO; *B* CH_2CHCH_3

[b] *A* CH_3CHO; *B* CH_2CH_2

2MO-TS_{II}), even though no similar states had previously been reported for oxetane [37]. Figure 1 shows the most salient features of the two stationary points.

The geometric similarity between the two species and those provided by the single-configuration methods (Fig. 1) led us to conclude that both saddle points must also correspond to concerted [2 *s* + 2 *s*] cycloreversion to 2-methyloxetane.

At the CASSCF level, the transition state 2MO-TS_I has a lower energy than 2MO-TS_{II} (Fig. 7), which is consistent with both experimental evidence and the results of the above-described single-determinant methods. However, introducing the dynamic correlation inverted the sequence. This seemingly inconsistent result is of little consequence since, as shown below, the prevalence of one reaction pathway over the other is not dictated by these transition states.

3.2.2 *Stepwise mechanisms IV and VI*

These mechanisms involve the initial cleavage of a C–C bond in 2-methyloxetane. Both processes proceed via a biradical species (2MO-INT_{IV} and 2MO-INT_{VI}) with

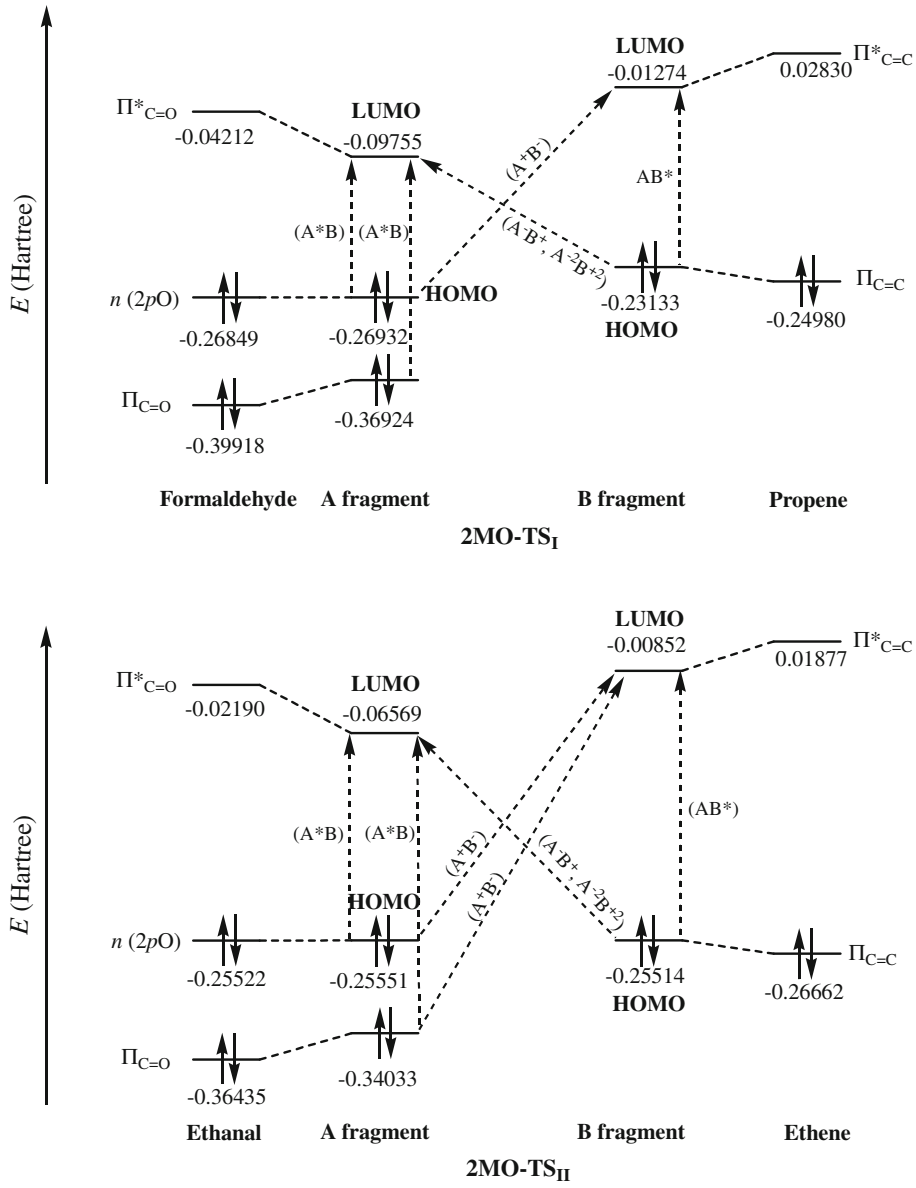

Fig. 3 Frontier molecular orbitals electronic energies of the products and these values when they place in position (considered as fragments) in the transition states 2MO-TS_I and 2MO-TS_{II}, electronic transfers between the MOs (*dashed arrows*) and the configurations they giving rise (in parentheses), according to analysis results of the configurational wavefunctions performed with the B3LYP/6-31G(d) theoretical model

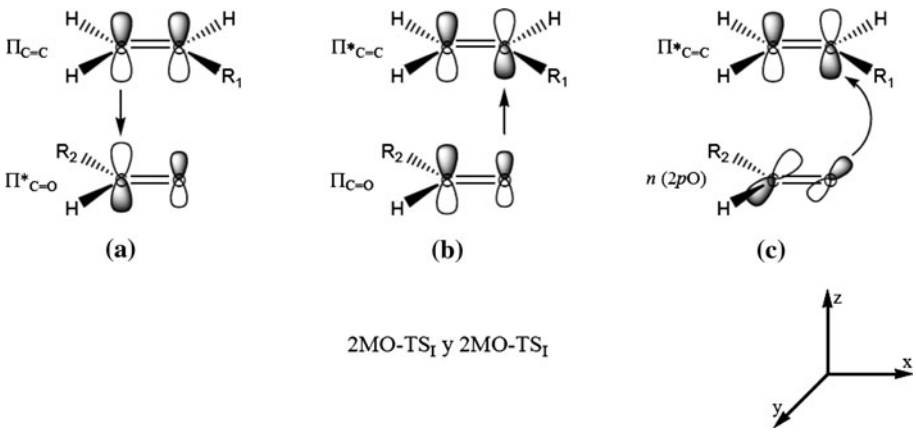

Fig. 4 Interactions between frontier molecular orbitals in 2MO-TS_I and 2MO-TS_{II}. $R_1 = CH_3$ in 2MO-TS_I, H in 2MO-TS_{II}, $R_2 = H$ in 2MO-TS_I, CH_3 in 2MO-TS_{II}

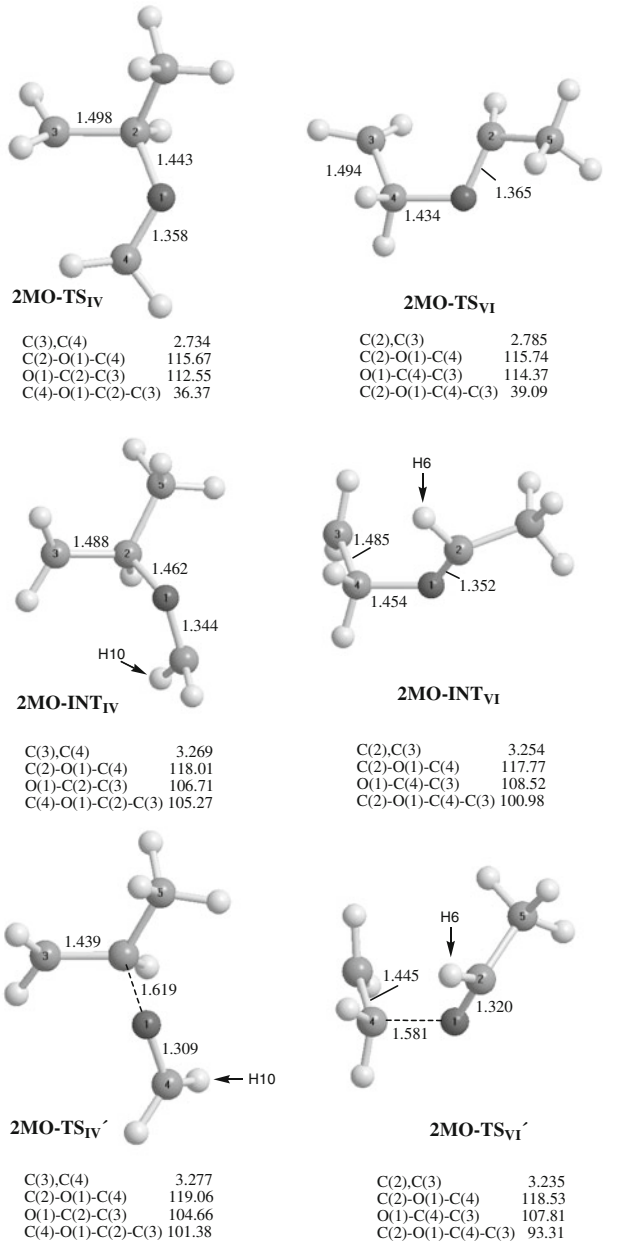

Fig. 5 Most important geometric parameters of stationary points for the paths IV and VI obtained with the CASSCF(6,5)/6-31G (d) theoretical model. Bond distances are given in Å and angles in degrees

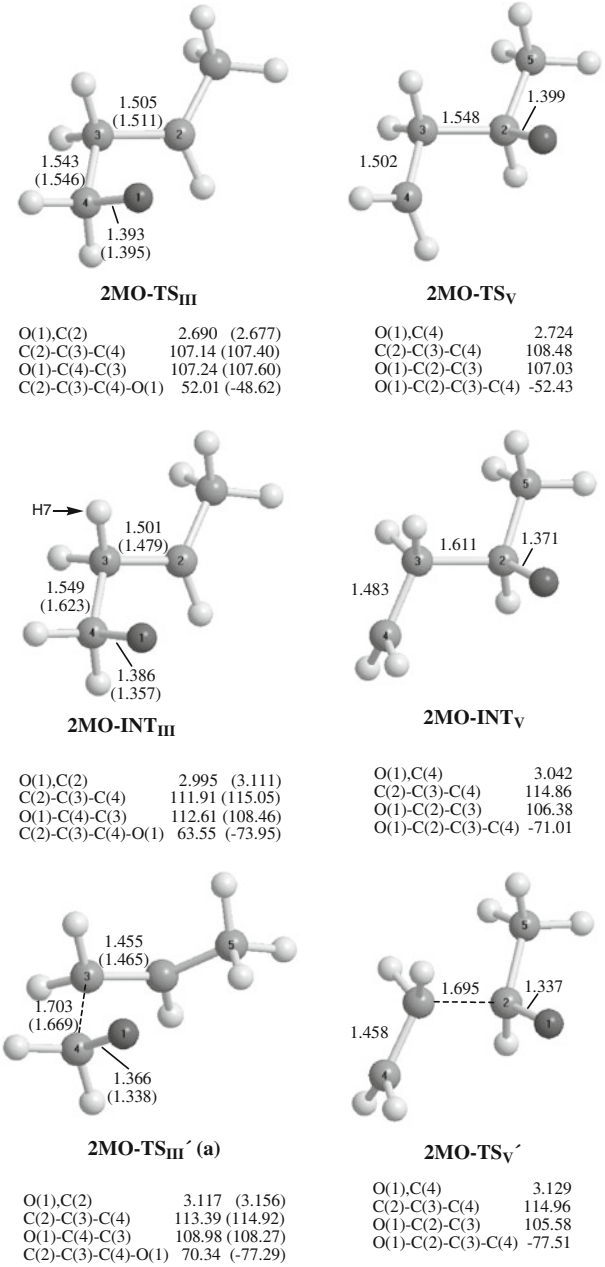

Fig. 6 Most important geometric parameters of stationary points for the paths III and V obtained with the CASSCF(6,5)/6-31G (d) theoretical model. Bond distances are given in Å and angles in degrees. **a** For 2MO-TSIII, 2MO-INTIII and 2MO-TSIII′, the data *not in parentheses* correspond to the gauche-in conformational isomers, and those that in *parentheses* correspond to the gauche-out rotamers. **b** The values for 2MO-TSIII′ (gauche-in) correspond to the CASSCF(6,5)/6-31G model

radical sites in two carbon atoms—both of which were located in the CASSCF(6,5)/6-31G(d) potential surface energy, as well as the transition states connecting the intermediates with both reagent and reaction products. Based on the way the radical sites are arranged, these two species are *gauche* conformers—the only ones which can be directly obtained by initial cleavage of the ring. Also for these intermediate structures, both may undergo rotation of the fragments about the still intact C–O bond in order to adopt the corresponding *anti* conformation rather than evolving to the 2-methyloxetane or to the respective set of reaction products. However, we chose not to explore these potential pathways since they were mere indirect routes to the same end products.

Going from reaction products to the 2-methyloxetane, 2MO-TS$_{IV'}$ and 2MO-TS$_{VI'}$ are the saddle points

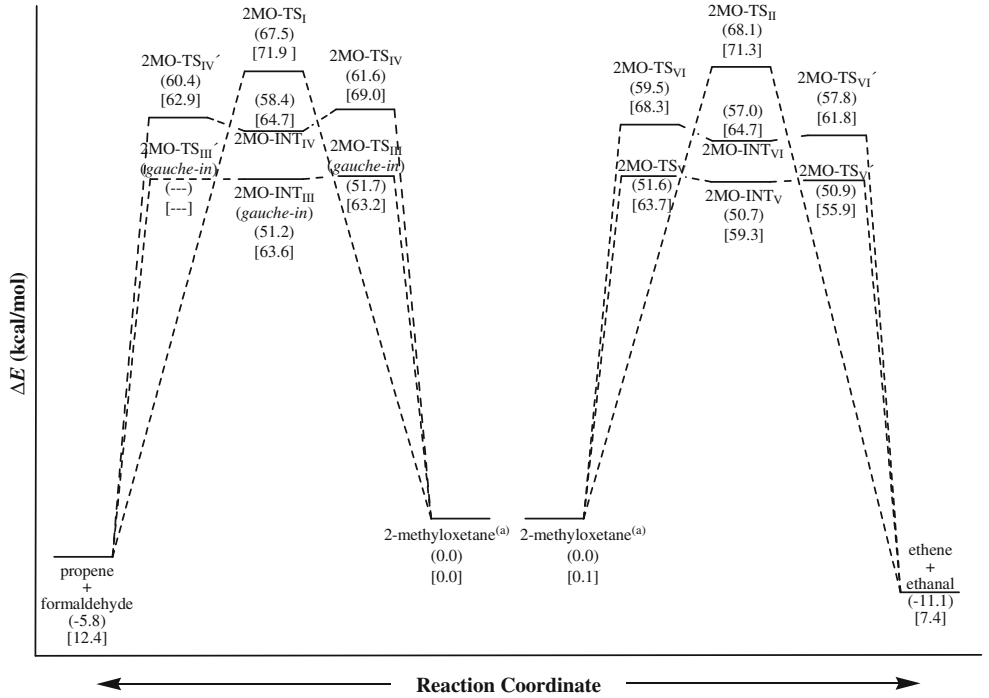

Fig. 7 Reaction energy profiles corresponding to the CASSCF(6,5)/6-31G(d)//CASSCF(6,5)/6-31G(d) (*in parentheses*) and CASPT2(8,8)/cc-pvDZ//CASSCF(6,5)/6-31G(d) (*in brackets*)

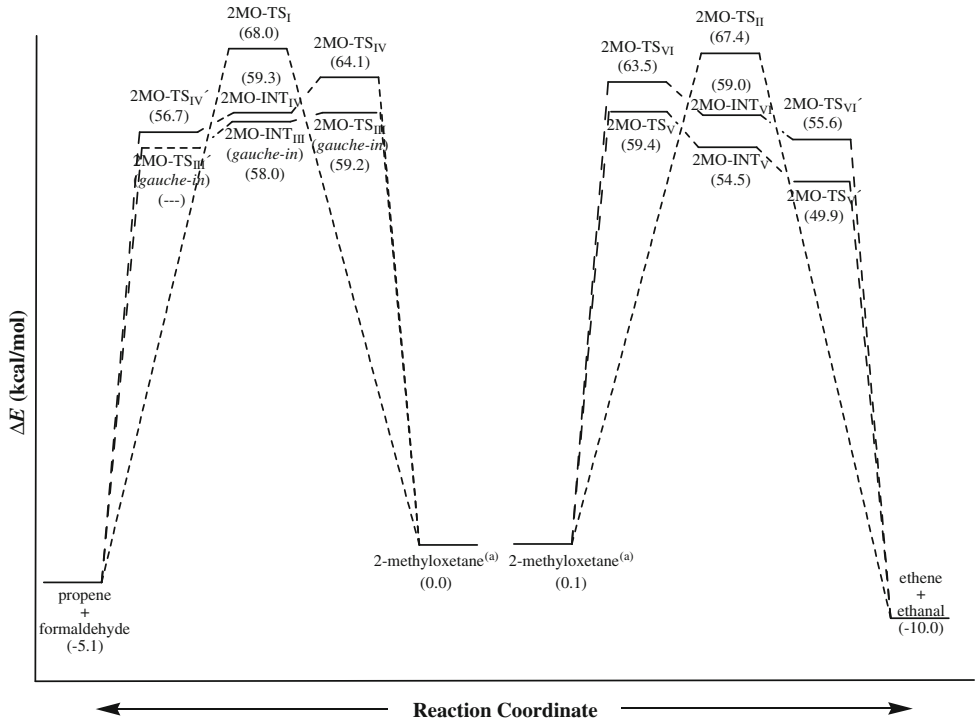

Fig. 8 Reaction Gibbs free energy profiles corresponding to the CASPT2(8,8)/cc-pvDZ//CASSCF(6,5)/6-31G(d) calculations

connecting the respective set of reaction products with the local minima 2MO-INT$_{IV}$ or 2MO-INT$_{VI}$. 2MO-TS$_{IV'}$ and 2MO-TS$_{VI'}$ have a C–O bond distance of 1.619 and 1.581 Å, respectively (Fig. 5). The interacting fragments in these structures, with a C_2–O_1–C_4–H_{10} dihedral angle of 35.19° in the former and a C_4–O_1–C_2–H_6 angle of 41.04° in the latter, must adopt a configuration midway between (a) one attack of the aldehyde to the alkene with the two

fragments in parallel and a C_2–O_1–C_4–H_{10} dihedral angle of ca. 90° (this rearrangement correlating with the ground state of both interacting fragments), and (b) another with the fragments lying normal to each other and a C_4–O_1–C_2–H_6 dihedral angle of c.a. 0°(that correlates with a n ($2p$O) → $\Pi^*_{C=O}$ excited state for the formaldehyde fragment, i.e. with the first excited singlet state). Therefore, although both transition states correspond to the lowest-energy PES, the CASSCF wavefunctions for these structures include not only the configuration for the ground state—that with the greatest weight—but also one other with a substantial weight with the aldehyde in an n-Π^* excited state. Because the two stationary points fall at a relative maximum of reaction coordinate on the ground singlet PES, but are typical of species on an excited-state PES, both surfaces must be very close in the respective regions of the PES. In consequence, transition states connecting both gauche minima with their products must correspond to avoid crossing points, as previously found in an MC-SCF study of the Paternò–Büchi reaction [37]. For 2MO-TS_{IV} and 2MO-TS_{VI}, we can make similar considerations.

3.2.3 Stepwise mechanisms III and V

The fragmentation process may also evolve via one biradical with a radical site in one carbon atom and another in the oxygen atom, i.e. via the 2MO-INT_{III} or 2MO-INT_V intermediates. Pathway III was examined as regards routes involving both *gauche-in* and *gauche-out* conformers. Because the route involving *gauche-in* conformers had a lower energy profile than that involving *gauche-out* conformers, only the former is described here (Fig. 6 depicts both). All species belonging to the three reaction pathways depicted at the left part of Scheme 2 were located on the CASSCF(6,5)/6-3G(d) PES; by exception, the transition state 2MO-$TS_{III'}$ (*gauche-in*) had to be optimized only with the 6-31G basis set.

2MO-$TS_{III'}$ and 2MO-$TS_{V'}$ are the transitions states reached by fragmentation of the C–C bond in the biradical intermediates 2MO-INT_{III} (*gauche-in*) and 2MO-INT_V, respectively. The C–C bond length at these saddle points is 1.703 and 1.695 Å, respectively, both of which exceed those for their originating intermediates. The long distance between the radical sites (3.117 Å in 2MO-$TS_{III'}$ and 3.129 Å in 2MO-$TS_{V'}$) is suggestive of absence of mutual interaction at this stage of the fragmentation.

2MO-INT_{III} (*gauche-in*) and 2MO-INT_V are the biradical intermediates formed in the initial cleavage of the C–O bond in 2-methyloxetane. As can be seen, the C_5–C_2–C_3–H_7 dihedral angle changes from 2.73° in 2-methyloxetane to −45.01° in 2MO-INT_{III} (*gauche-in*) and −68.73° in 2MO-INT_V, thereby avoiding the relative eclipsed position of the C3-H7 and C2-Me bonds on the initial heterocycle. As it was stated by Robb et al. [37], the two lower potential energy surfaces for the biradical intermediates 2MO-INT_{III} or 2MO-INT_V can be exchanged by *orbital rotation* at the oxygen atom [37]; therefore, the wavefunctions describing the species involved in pathways III and V also may include some contribution from excited states, as was the case with pathways IV and VI by *geometric rotation* of the oxygen-bonded terminal methylene group.

2MO-TS_{III} (*gauche-in*) and 2MO-TS_V are the transition states for the initial cleavage of the C–O bond on the ring and connect the reagent with the intermediates 2MO-INT_{III} (*gauche-in*) and 2MO-INT_V, respectively. In these species, the C–C bond is completely formed—it is 1.543 Å long in 2MO-TS_{III} (*gauche-in*) and 1.548 Å in 2MO-TS_V— also, the torsional angle about the C–C bond is still very low (52.01° and −52.43°, respectively). The distance between radical sites is about 2.700 Å, which is suggestive of a weak interaction between unpaired electrons.

3.2.4 Analysis of the energy profile for the thermolytic reaction

In this section, we will discuss the energy characteristics of the species described in the previous two. Figure 7 shows the CASSCF(6,5)/6-31G(d)//CASSCF(6,5)/6-31G(d) (in parentheses) and CASPT2(8,8)/cc-pvDZ//CASSCF(6,5)/6-31G(d) (in brackets) relative energies. To take into account entropic effects, we also represented in Fig. 8 the Gibbs free energy profiles obtained from our CASPT2(8,8)/cc-pvDZ//CASSCF(6,5)/6-31G(d) results that for this approach corrects the atypical relative position of the 2MO-INT_{III} level in Fig. 7. No results for the *gauche-out* conformers of the species involved in pathway III (Scheme 2) have been included since 2MO-TS_{III} (*gauche-in*) was 1.6 kcal/mol more stable than 2MO-TS_{III} (*gauche-out*). As can be seen, the transition states of the synchronous and concerted processes (2MO-TS_I and 2MO-TS_{II}) exhibited high energy values than every species involved in the stepwise pathways of Scheme 2; therefore, the thermally induced decomposition of 2-methyloxetane must primarily take place in a asynchronous mode and, if are right the CASSCF predictions, involving biradical intermediates. These results should be consistent with previous findings of Holbrook et al. [30] for oxetane that the rate-determining kinetic step in the stepwise fragmentation reaction is that involving the formation of a biradical. As can also be seen, the CASSCF energy profiles are very flat in the biradical regions; the barriers to be overcome on both sides of the biradical intermediates can be assigned to the slight steric changes occurring while the system rotates about the C–O bond in 2MO-TS_{IV} and 2MO-INT_{VI} or the C–C bond in 2MO-INT_{III} and 2MO-INT_V. However, activation energy

barriers for the overall reactions were underestimated by CASSCF in comparison with available experimental values (and also probably was overestimated the stability of biradicals).

Also apparent from the figure is that considering the effects of dynamic correlation leads to the biradical intermediates—2MO-$TS_{III'}$ (*gauche-in*) excepted as it could not be located—appearing with higher energy than the transition states for the second step of fragmentations, i.e. when dynamical effects were considered biradicals become unstable, and therefore, the favorable paths should be "concerted asynchronous" instead stepwise, i.e. once the first bond is practically broken, their connection with the fragments is subject to no other energy barrier and the process continues very rapidly.

These results can be attributed to the almost flat form of the energetic profile of biradical area and the presumably error derived from carried out single points CASPT2(8,8)/cc-pVDZ energy calculations for CASSCF(6,5)/6-31G(d) geometries which are not necessarily stationary points—but, presumably, close—on the CASPT2(8,8)/cc-pVDZ PES. More investigations must be derived in this respect and so the exact mechanism remains still an open question. Nonetheless, our CASPT2//CASSCF results show a good agreement with experimental activation energies, especially for the more favorable paths (*MUE = 2.9,* if we compare the estimated activation enthalpies (59.20 and 59.29 kcal/mol) with the respective data from Zalotai, although CASPT2//CASSCF energetic predictions are in better accordance with the Holbrook's statement of two competitive reactions with similar activation energy barriers).

The lowest-energy pathways are those involving the initial cleavage of the C–O bond in 2-methyloxetane, the energy for the transition state 2MO-TS_{III} (*gauche-in*), which undergoes cleavage of the C_2–O_1 bond being slightly lower (0.5 kcal/mol) than that for 2MO-TS_V—where the C_4–O_1 bond is broken. This route evolves to propene and formaldehyde, which are the experimentally known reaction products for the main reaction pathway [29, 35]. From Gibbs activation energies for the two more favorable competitive reaction channels, we predict a 60% relative yield of the reaction channel via 2MO-TS_{III} against the channel 2MO-TS_V (being negligible the contributions of synchronous paths and others to global reaction rates).[1] So our CASPT2//CASSCF predicted branching ratio is comparable with the experimental value of ca. 1.3 [35].

One of the potential reasons for pathways III and V being more stable than IV and VI, respectively, would be the slight eclipsed position of the oxygen-bonded radical fragment in the area of biradical intermediates 2MO-INT_{IV} and 2MO-INT_{VI} (viz. the methylene group in the former and the ethylene group in the latter) and the C_2-bonded hydrogen atom (or C4-bonded in the 2MO-INT_{VI} specie)—which should be absent from the biradicals 2MO-INT_{III} (*gauche-in*) and 2MO-INT_V. The pathway III resulting more stable than the V can be understand taking in consideration the reverse cycloaddition process: in this point, the $+I$ character of the C_2-bonded methyl group favors the attack of propene to formaldehyde, which occurs via C_3 and C_4, over the attack of the ethene to ethanal (where this inductive effect hinders the attack of the aldehyde by the alkene); in addition, the still hypothetical intermediate for the former case, the 2MO-INT_{III} (gauche-in), must be more stable than the 2MO-INT_V by virtue of hyperconjugative effects of that specie (the bonding of the methyl group to C2 stabilizes its radical site).

4 Conclusions

The results obtained in this work warrant the following comments by way of summary:

1. Applying the single-configuration methods MP2, B3LYP and MPW1K to the two possible fragmentation pathways for the thermolysis of 2-methyloxetane led to highly synchronous concerted mechanisms and the absence of biradical species on the explored PES (as exception, trial UB3LYP calculations drove to some isolated stationary points but not to the complete set of species that collects the Scheme 2). The preferential cleavage of the C–O bond relative to the C–C bond, together with the presence of geometric distortion in the transition states, facilitates interactions of the *supra–supra* type between fragments. The energy of the transition state for the highly synchronous concerted process leading to propene and formaldehyde (2MO-TS_I) is slightly lower than that of the saddle point 2MO-TS_{II}—QCISD(T)-FC/cc-pvDZ//B3LYP/6-31G(d) calculations excepted—which connects the reagent with ethene and ethanal.
2. The CASSCF multi-configuration methods (6 electrons/5 orbitals) allowed four different reaction pathways involving biradical intermediates to be identified; two such pathways involve initial cleavage of the C–C bond and two cleavage of the C–O bond. All four involve *gauche* isomers as regards arrangement of the two radical sites and have wavefunctions including some contribution from excited states. The two

[1] The relative yield for reaction I of Scheme 1 was estimated according the following formula:

$$\% = \frac{\exp\{-\Delta G^{\neq}(TS_{III})/RT\}}{\exp\{-\Delta G^{\neq}(TS_{III})/RT\} + \exp\{-\Delta G^{\neq}(TS_V)/RT\}} 100.$$

additional transition states directly connecting the reagent with two potential sets of products were also located but with higher activation energies that the stepwise paths. However, biradical intermediates become unstable by including the dynamical effects by single point CASPT2(8,8)/cc-pvDZ//CASSCF(6,5)/6-31G(d) calculations, and so the thermal fragmentation of 2-methyloxetane should be primarily an asynchronous process in which activation energies principally arise of breaking of the first of the two bonds to be broken. Particularly, the pathway via the 2MO-TS $_{III}$ (*gauche-in*) is that subject to the lowest-energy barrier among those involving fragmentation of the ring. Once overpasses the 2MO-TS$_{III}$ (*gauche-in*), the supermolecule rapidly evolves to propene and formaldehyde, which are the experimentally detected products of the main reaction pathway. Good accordance was obtained between CASPT2//CASSCF results and some experimental evidences as activation energies and the branching ratio for the two competitive processes.

3. The PES is so flat at the region of interest (biradical and TS′s) that results are very sensitive to the employed theoretical method. For this reason, both the CASSCF and the DFT schemes apparently reach their respective limits of applicability due to an imbalance in their treatment of the two types of electron correlation. A definitive conclusion about the true nature of mechanism requires more investigations.

References

1. Schreiber SL, Satake K (1983) J Am Chem Soc 105:6723
2. Schreiber SL, Hoveyda AH (1984) J Am Chem Soc 106:7200
3. Bach T (1997) Liebigs Annalen 1997:1627
4. Bach T, Schröder J (1997) Tetrahedron Lett 38:3707
5. Bach T (1998) Synthesis 5:683
6. Bach T, Bergmann H, Brummerhop H, Lewis W, Harms K (2001) Chem Eur J 7:4512
7. Jones G II, Schwartz SB, Marton MT (1973) J Chem Soc Chem Commun 11:374
8. Jones G II, Kleinman HH (1974) Tetrahedron Lett 15:2103
9. Jones G II, Acquadro MA, Carmody MA (1975) J Chem Soc Chem Commun 6:206
10. Miranda MA, Izquierdo MA, Galindo F (2001) Org Lett 3:1965
11. Miranda MA, Izquierdo MA, Galindo FJ (2002) Org Chem 67:4135
12. Miranda MA, Izquierdo MA (2002) J Am Chem Soc 24:6532
13. Nakabayashi K, Kojima JI, Tanabe K, Yasuda M, Shima K (1989) Bull Chem Soc Jpn 62:96
14. Prakash G, Falvey DE (1995) J Am Chem Soc 117:11375
15. Joseph A, Prakash G, Falvey DE (2000) J Am Chem Soc 122:11219
16. Joseph A, Falvey DE (2001) J Am Chem Soc 123:3145
17. Joseph A, Falvey DE (2002) Photochem Photobiol Sci 1:632
18. Song QH, Hei X, Xu Z, Zhang X, Guo Q (2003) Bioorg Chem 31:357
19. Wang Y, Gaspar PP, Taylor JS (2000) J Am Chem Soc 122:5510
20. Cichon MK, Arnold S, Carell T (2002) Angew Chem Int Ed 41:767
21. Carell T, Burgdorf LT, Butenandt J, Epple R, Schwogler A (1999) Bioorg Chem 242
22. Stafforst T, Diederichsen U (2005) Chem Comm 27:3430
23. Sancar A (2003) Chem Rev 42:6747
24. Kim S-T, Malhorta K, Smith CA, Taylor JS, Sancar A (1994) J Biol Chem 269:8535
25. Kim S-T, Malhorta K, Smith CA, Taylor JS, Sancar A (1996) Photochem Photobiol 63:292
26. Hitomi K, Nakamura H, Kim S-T, Mizukoshi T, Ishikawa T, Iwai S, Todo T (2001) J Biol Chem 276:10103
27. Clivio P, Fourrey J-L (1998) Tetrahedron Lett 39:275
28. Heelis PF, Liu S (1997) J Am Chem Soc 119:2936
29. Zalotai L, Bérces T, Márta F (1990) JCS Faraday Trans 86(1):21
30. Holbrook KA, Scott RA (1975) JCS Faraday Trans I 71:1849
31. Bittker DA, Walters WD (1955) J Amer Chem Soc 77:1429
32. Carless HAJ (1974) Tetrahedron Lett 38:3425
33. Holbrook KA, Scott RA (1974) JCS Faraday Trans I 70:43
34. Chow N, Wilson DJ (1962) J Phys Chem 66:342
35. Holbrook KA, Oldershaw GA, Shaw CJ, Dyer PE (1989) JCS Faraday Trans 2 85(6):597
36. Carless HAJ, Maitra AK, Pottinger R, Frey HM (1980) JCS Faraday Trans I 76:1849 (and references therein)
37. Palmer IJ, Ragazos IN, Bernardi F, Olivucci M, Robb MA (1994) J Am Chem Soc 116:2121
38. Calvo-Losada S, Enríquez F, Martín-Ortiz J, Quirante JJ (2003) J Phys Chem A 107(16):2919
39. Roos BO, Taylor PR, Siegbahn PEM (1980) Chem Phys 48:157
40. Roos BO, Linse P, Siegbahn PEM, Blomberg RA (1982) Chem Phys 66:197
41. Roos BO (1987) In: Lawley KP (ed) Advances in chemical physics; Ab initio methods in quantum chemistry-II. Wiley, Chichester
42. Parr RG, Yang W (1989) Density functional theory of atoms and molecules. Oxford University Press, New York
43. Kohn W, Becke AD, Parr RG (1996) J Phys Chem 100:12974
44. Orlova G, Goddard JD (2000) J Chem Phys 112:10085 and references therein
45. Staroverov VN, Davidson ER (2001) J Mol Struct (THEOCHEM) 573:81
46. Martin J (2010) PhD Thesis. University of Málaga
47. Houk KN, Beno BR, Nendel M, Black K, Yoo HY, Wilsey S, Lee JK (1997) J Mol Struct (Theochem) 398–399:169
48. Goldstein E, Beno BR, Houk KN (1996) J Am Chem Soc 118:6036
49. Cremer D, Kraka E, Szalay PG (1998) Chem Phys Lett 292:97
50. He Y, Gräfenstein J, Kraka E, Cremer D (2000) Mol Phys 98:1639
51. Gräfenstein J (2000) Cremer D Phys Chem 2:2091
52. Gräfenstein J, Hjerpe A, Kraka E, Cremer D (2000) J Phys Chem A 104:1748
53. Wiest O, Montiel DC, Houk KN (1997) J Phys Chem A 101: 8378
54. Jarzecki AA, Gajewski J, Davidson ER (1997) J Am Chem Soc (1999) 121:6928
55. Becke AD (1988) Phys Rev B 38:3098
56. Becke AD (1993) J Chem Phys 98:5648
57. Lee C, Yang W, Parr RG (1988) Phys Rev B 37:785
58. Lynch BJ, Fast PL, Harris M, Truhlar DG (2000) J Phys Chem A 104:4811
59. Andersson K, Roos BO (1995) In: Yarkony DR (ed) Modern electronic structure theory. World Scientific, Singapore

60. Gaussian 03, Revision B.04, Frisch MJ, Trucks GW, Schlegel HB, Scuseria GE, Robb MA, Cheeseman JR, Montgomery JA Jr, Vreven T, Kudin KN, Burant JC, Millam JM, Iyengar SS, Tomasi J, Barone V, Mennucci B, Cossi M, Scalmani G, Rega N, Petersson GA, Nakatsuji H, Hada M, Ehara M, Toyota K, Fukuda R, Hasegawa J, Ishida M, Nakajima T, Honda Y, Kitao O, Nakai H, Klene M, Li X, Knox JE, Hratchian HP, Cross JB, Adamo C, Jaramillo J, Gomperts R, Stratmann RE, Yazyev O, Austin AJ, Cammi R, Pomelli C, Ochterski JW, Ayala PY, Morokuma K, Voth GA, Salvador P, Dannenberg JJ, Zakrzewski VG, Dapprich S, Daniels AD, Strain MC, Farkas O, Malick DK, Rabuck AD, Raghavachari K, Foresman JB, Ortiz JV, Cui Q, Baboul AG, Clifford S, Cioslowski J, Stefanov BB, Liu G, Liashenko A, Piskorz P, Komaromi I, Martin RL, Fox DJ, Keith T, Al-Laham MA, Peng CY, Nanayakkara A, Challacombe M, Gill PMW, Johnson B, Chen W, Wong MW, Gonzalez C, Pople JA (2003) Gaussian, Inc., Pittsburgh PA
61. Karlström G, Lindh R, Malmqvist P-Å, Roos BO, Ryde U, Veryazov V, Widmark P-O, Cossi M, Schimmelpfennig B, Neogrady P, Seijo L (2003) Comput Mater Sci 28:222
62. Schlegel HB (1982) J Comp Chem 3:214
63. Fukui K (1981) Acc Chem Res 14:363
64. González C, Schlegel HB (1990) J Phys Chem 94:5523
65. Fujimoto H, Kato S, Yamabe S, Fukui K (1974) J Chem Phys 60:572
66. Kato S, Fujimoto H, Yamabe S, Fukui K (1974) J Am Chem Soc 96:2024
67. Menéndez MI, Sordo JA, Sordo TL (1992) J Phys Chem 96:1185
68. López R, Menéndez MI, Suárez D, Sordo TL, Sordo JA (1993) Comput Phys Commun 76:235
69. Menéndez MI, González J, Sordo JA, Sordo TL (1994) J Mol Struct (Theochem) 309:295 and references therein
70. Suárez D, Sordo TL, Sordo JA (1995) J Org Chem 60:2848
71. Mayer I (1986) Int J Quant Chem 29:73
72. Mayer I (1986) Int J Quant Chem 29:477